Processing and Application of Ceramics 12 [2] (2018) 136–142
https://doi.org/

Highly porous hydroxyapatite derived from cuttlefish bone as TiO_2 catalyst support

Dajana Milovac[1,*], Ivna Weigand[2], Marin Kovačić[1], Marica Ivanković[1], Hrvoje Ivanković[1]

[1]*University of Zagreb, Faculty of Chemical Engineering and Technology, Zagreb, Croatia*
[2]*Institute IGH, Zagreb, Croatia*

Received 12 December 2017; Received in revised form 21 March 2018; Accepted 15 May 2018

Abstract

Highly porous hydroxyapatite ($Ca_{10}(PO_4)_6(OH)_2$, HAp) catalyst support was prepared through hydrothermal transformation of aragonitic cuttlefish bone (Sepia Officinalis, L., Adriatic Sea) at 200 °C, preserving the natural well interconnected porous structure. To deposit the TiO_2 catalyst on the pore walls of the HAp support two methods were used: i) vacuum impregnation of the support with the suspension of a commercial TiO_2 nanopowder in isopropanol and ii) in situ synthesis of TiO_2 on the support by sol-gel technique. XRD analysis and FTIR spectroscopy were used to determine the phase composition of the material. The morphology and microstructure of the composite samples were studied by scanning electron microscopy (SEM). The presence of TiO_2 particles on the HAp surface was determined by SEM/EDX analysis. To determine the specific surface area and pore size, Brunauer-Emmett-Teller (BET) method was used. The results of the BET method showed the increased specific surface area and pore size reduction after impregnation of TiO_2 into the HAp carrier. The photocatalytic activity of HAp/TiO_2 samples was studied in a batch reactor with an annular UV-A lamp using salicylic acid as a model water pollutant. The results indicated the suitability of prepared HAp supported TiO_2 catalysts for photocatalytic applications.

Keywords: *hydroxyapatite, TiO_2, impregnation, sol-gel process, photocatalysis*

I. Introduction

Highly porous ceramics are broadly used in different catalytic processes as catalysts or catalyst supports. Besides good thermal and chemical stability and mechanical strength, high surface area and good pore connectivity are crucial for the catalyst performance. In the last decade, a great deal of research has been focused on the development of new types of catalyst support based on alumina and cordierite [1–3], zeolites [4], silicon-carbide [5], and metal oxides, such as TiO_2 [6], La_2O_3, CeO_2, MnO_2 and ZrO_2 [7].

Recently, the potential of biomaterials such as hydroxyapatite, HAp, as catalyst support has been recognized. Few interesting applications in heterogeneous catalysis, e.g. CO oxidation and oxidative esterification of aldehydes [8,9] emerged so far. Relatively little attention has been paid in the literature to the utilization of hydroxyapatite derived from natural porous materials as catalyst support. Chakraborty *et al.* [10–12] reported on successful application of hydroxyapatite derived from fish bone as a support for preparation of low-cost, recyclable, heterogeneous catalysts. Very recently, TiO_2 has been immobilized onto 3D spongin-based scaffolds isolated from *H. communis* marine demosponge [13].

In our previous studies [14–16] highly porous HAp scaffold, for bone tissue engineering applications, has been prepared from cuttlefish bone. Cuttlefish bone is a low cost, worldwide available natural cellular material possessing high stiffness, high porosity (~90%) and high permeability. Natural aragonite from cuttlefish bone was hydrothermally transformed into HAp at 200 °C preserving the natural well interconnected porous structure. The results obtained in these studies motivated us to examine the potential of this 3D porous natural architecture, which might be difficult to produce artificially, as catalyst support. We hypothesized that such structure would ensure a high surface area of immobilized catalyst and good mass transport of the pol-

* Corresponding author: tel: +385 1 4597 226,
e-mail: *dmilovac@fkit.hr*

lutants to the catalyst surface.

Titanium dioxide (TiO_2) is one of the most efficient semiconductor catalysts which exhibits a high efficiency in the photo-oxidation of undesired and harmful air contaminants [17–19] and water pollutants [20,21]. TiO_2 exists in nature in three different polymorphs, namely, rutile, anatase and brookite. Only anatase and rutile are photocatalytically active. Anatase is widely used in photocatalysis due to its favourable band gap energy (3.2 eV), commercial availability, relatively inexpensive cost, non-toxicity and high photochemical stability. Being exposed to UV light, large amount of reactive oxygen species, such as hydroxyl radicals ($OH^{\bullet}$) and superoxide radical anion ($O_2^{\bullet}$), are produced on the surface of TiO_2. These reactive radicals are regarded as the major species responsible for the degradation of pollutants into CO_2 and H_2O. A common approach to enhance the photocatalytic activity of TiO_2 is to increase its surface area using TiO_2 in the form of nanoparticles. However, for applications in water, such small suspended particles require high filtration costs for catalyst removal once the reaction is finished. These problems led to the development of supported photocatalysts in which TiO_2 has been immobilized on porous materials with a high surface area.

In this work, a TiO_2 photocatalyst was deposited on the pore walls of the HAp support derived from cuttlefish bone. Two methods were used: i) vacuum impregnation of the support with the suspension of a commercial TiO_2 powder in isopropanol and ii) *in situ* synthesis of TiO_2 on the support by sol-gel technique. The photocatalytic activity of the prepared catalyst was studied using salicylic acid as a model water pollutant and compared to that of suspended TiO_2 nanoparticles.

II. Experimental

2.1. Preparation of HAp/TiO$_2$ composite

Cuttlefish bones (*Sepia officinalis*, L.) from the Adriatic Sea were used as starting material for the hydrothermal synthesis of hydroxyapatite (HAp). The bones were carefully cut into small pieces and treated with an aqueous solution of sodium hypochlorite (NaClO, 13% active chlorine, Gram-mol) for 12 h at room temperature to remove the organic component. The pieces of cuttlefish bone were then sealed with the required volume (respecting the molar ratio of Ca/P = 1.67) of a 0.6 M aqueous solution of ammonium dihydrogenphosphate ($NH_4H_2PO_4$, 99%, Scharlau) in a TEFLON lined stainless steel pressure vessel at 200 °C for 72 h. The pressure inside the reactor was self-generated by water vapour and reached 18 bar. After hydrothermal treatment the resulting HAp scaffolds were washed with boiling demineralized water, dried at 105 °C, annealed at 500 °C for 1 h, and characterized. The dried samples are denoted as HAp, 105 °C, and the annealed samples are denoted as HAp.

Highly porous HAp pieces were impregnated with a 5 wt.% suspension of titanium dioxide (TiO_2, P25, Degussa) in isopropanol (2-propanol, 99%, Gram-mol) using the vacuum impregnation unit (Citovac Struers). The purpose of vacuum impregnation is the removal of air from the samples for complete penetration of TiO_2 suspension in the pores of HAp. After the vacuuming, the samples of HAp were kept immersed in TiO_2 suspension for 30 min. The soaked samples were put on a net and placed in the vacuum chamber again in order to remove the excess of TiO_2 suspension away from the scaffolds. The impregnated samples were dried at 105 °C, annealed at 500 °C for 1 h, and characterized. The dried samples are denoted as HAp/TiO_2 (P25), 105 °C, and the annealed samples are denoted as HAp/TiO_2 (P25).

The second group of HAp/TiO_2 samples was prepared by vacuum impregnation of precursors exhibiting sol-to-gel transition into TiO_2. Titanium (IV)-isopropoxide, (TTIP, 97%, Aldrich) was added to 2-propanol (Gram-mol) and the mixture was stirred using a magnetic stirrer. Peptization agent, acetylacetone, (Ac-Ac ($CH_3C(O)CH_2C(O)CH_3$), 98%, Fluka) was added to the mixture and the molar ratio of Ac-Ac/TTIP was 0.3. In order to catalyse hydrolysis, a mixture of 1 M HNO_3 and 2-propanol was added to the TTIP/n-propanol mixture dropwise. After vigorous stirring at room temperature for 1 h, a transparent yellowish solution was obtained and the impregnation of the HAp carrier was performed as previously described. The resulting samples of impregnated HAp were then kept at room temperature overnight. To prepare the catalyst with TiO_2 content similar to that in HAp/TiO_2 (P25) catalyst the impregnation procedure and drying were repeated four times. The dried products were calcined at 500 °C for 1 h and denoted as HAp/TiO_2 SG.

2.2. Characterization methods

The prepared samples were structurally characterized by X-ray diffraction analysis (Shimadzu 6000) equipped with CuK_α radiation source at 40 kV and 30 mA in 2θ range from 5° to 70°, with a step of 0.02°/s. Identification of the phases was performed by comparing the experimental XRD patterns to standards compiled by JCPDS. XRD profile fittings and Rietveld refinements were performed using TOPAS V5 (Bruker AXS). Crystallite sizes were determined using the integral breadth (Lvol-IB) method. To quantify TiO_2 phase in the HAp/TiO_2 composite the standard addition method was used as well.

The Fourier transform infrared (FTIR) spectra of the materials were recorded by attenuated total reflectance (ATR) spectrometer for solids with a diamond crystal (Bruker VERTEX 70). An amount of a material was placed in the mortar and ground with the pestle for one minute and then put onto a diamond crystal. 64 scans were collected for each measurement over the spectral range of 400–4000 cm^{-1} with a resolution of 1 cm^{-1}.

Scanning electron microscopy (SEM) with energy

dispersive X-ray (EDX) analysis (SEM ISIDS-130) was used to examine the morphology of the raw cuttlefish bone, HAp and the HAp/TiO_2 composites. The samples were sputtered with gold three times.

The quantification of mesoporosity and microporosity was carried out according to the Brunauer-Emmett-Teller (BET) method by N_2 adsorption-desorption isotherms at liquid N_2 temperature on a Micrometrics ASAP 2000 instrument.

2.3. Photocatalytic test reaction

The photocatalytic properties of prepared catalyst have been studied by exposing the salicylic acid aqueous solution to UV light in the absence and in the presence of suspended pure TiO_2 (P25), suspended pure HAp or HAp supported TiO_2 photocatalysts. Preliminary dark experiments without irradiation were also performed to establish the period of time needed to achieve the adsorption-desorption equilibrium of all studied catalysts. Experiments were performed in a 125 ml cylindrical laboratory batch reactor made from Pyrex glass, mounted on a magnetic stirrer. A low-pressure mercury lamp with the primary emission output at 365 nm was used as the source of UV-A irradiation. The UV lamp was placed axially in a quartz tube inside the reactor. The following experimental conditions were kept constant throughout this study: 100 ml total volume, 0.2 mmol/l initial salicylic acid concentration. The amount of the added commercial TiO_2 (Degussa P25) photocatalyst, used as a reference, was 0.1 g/100 ml. The added amount of pure HAp or prepared HAp/TiO_2 composite catalysts was 1 g/100 ml. The solution was magnetically stirred (400 rpm) and adjusted to pH = 7.5. Prior to irradiation the solutions were kept in the dark for 30 min in order to establish adsorption equilibrium. After "dark" adsorption, the solutions were exposed to UV light. At different time intervals small aliquots (0.5 ml) of the solutions were taken out from the reactor, filtered and analysed for residual salicylic acid. The concentration of salicylic acid was determined using a LC-10 HPLC, Shimadzu, with an UV-DAD detector, equipped with Macherey-Nagel Nucleosil C18 column. The mobile phase consisted of 0.15% H_3PO_4 in water and methanol (50:50 v/v). The repeatability of photocatalytic activity of the HAp/TiO_2 (P25) photocatalyst was also tested. After the first photodegradation cycle the catalyst was separated from the treated solution, washed and dried. The separated catalyst denoted as HAp/TiO_2 (P25) II was added again to a new identical batch of salicylic acid solution and the degradation process was monitored as previously described. The efficiency of the salicylic acid mineralization was evaluated by measuring the total organic carbon (TOC) content with a Shimadzu, TOC-V_{CPN} analyser.

III. Results and discussion

3.1. XRD analysis

The phase composition of the prepared HAp/TiO_2 composites was determined by X-ray diffraction (XRD). The XRD patterns of HAp and HAp/TiO_2 composites are shown in Fig. 1.

The diffraction pattern of HAp derived from cuttlefish bone showed well-resolved peaks indicating a high degree of crystallinity of the inorganic material. Comparing the experimental diffraction pattern to JCPDS standards the crystalline phase was identified as hydroxyapatite mineral (JCPDS No. 09-0432). Besides the diffraction peaks belonging to HAp, the diffraction pattern of HAp/TiO_2 (P25) composite showed additional diffraction peaks at 2θ = 25.2°, 27.3°, 37.7°, 48.08°, 54.0° and 55° attributed to the anatase/rutile phase. All peaks are in good agreement with the standard spectrum (JCPDS No. 21-1272 and JCPDS No. 21-1276). According to the manufacturer's specifications, titanium dioxide (Degussa P25) has 80% anatase and 20% rutile phase. Our analysis of XRD data showed slightly different values: 84% anatase and 16% rutile phase. The existence of rutile in the nanopowder is discernible from its 110 diffraction peak located at 2θ of 27.3° in the XRD pattern. The HAp/TiO_2 SG powder pattern showed typical peaks of HAp and anatase. A very small amount of rutile phase is hardly seen in Fig. 1. The XRD data analy-

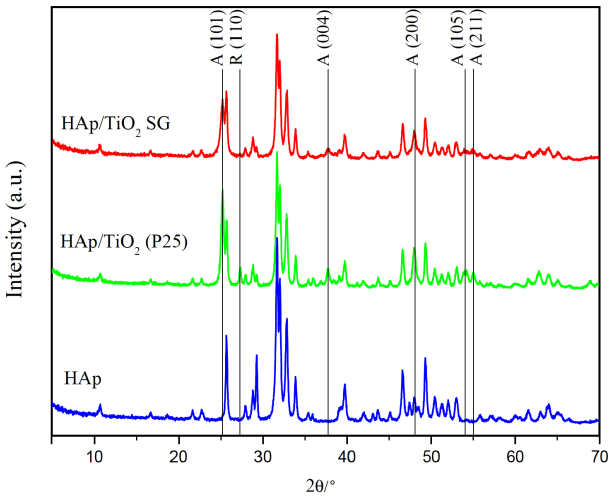

Figure 1. XRD patterns of HAp and HAp/TiO_2 composites (the vertical lines are the 2θ positions of anatase (A) and rutile (R) - for purpose of clarity, the HAp lines were not marked)

Table 1. Results of X-ray diffraction quantitative analysis

Sample	TiO_2 content [wt.%]	Anatase/rutile ratio [%]	Relative crystallite size [nm]	
			Anatase	Rutile
HAp/TiO_2 (P25)	20.23	84/16	19.8	32.2
HAp/TiO_2 SG	18.32	96/4	14.0	19.4

sis showed that TiO_2 SG has 96% anatase and 4% rutile phase.

The quantitative composition of the prepared HAp/TiO_2 composites, determined using the standard addition method, from the diffraction patterns of calibration mixtures with different amounts of added TiO_2, relative amounts of TiO_2 crystalline phases (anatase/rutile) and their nanometric crystallite size are given in Table 1.

3.2. FTIR spectroscopy

FTIR spectra of prepared materials are shown in Fig. 2. The FTIR spectrum of HAp shows typical bands for PO_4^{3-} at 470 cm^{-1} for ν_2 mode, 561 cm^{-1} and 601 cm^{-1} for ν_4 mode, 960 cm^{-1} for ν_1 mode and 1018 and 1083 cm^{-1} for ν_3 mode. The high intensity of the CO_3^{2-} derived bands at 871 cm^{-1} for ν_2 mode, and 1413 cm^{-1} and 1456 cm^{-1} for ν_3 mode, indicates that B-type substitution occurred during HAp synthesis [22]. Besides PO_4^{3-} and CO_3^{2-} groups, FTIR spectrum of HAp/TiO_2 (P25) composite shows an additional broad band in the area of 650–800 cm^{-1} attributed to the stretching of Ti–O bonds, and the band at ~440 cm^{-1} attributed to the stretching of Ti–O–Ti bonds [23].

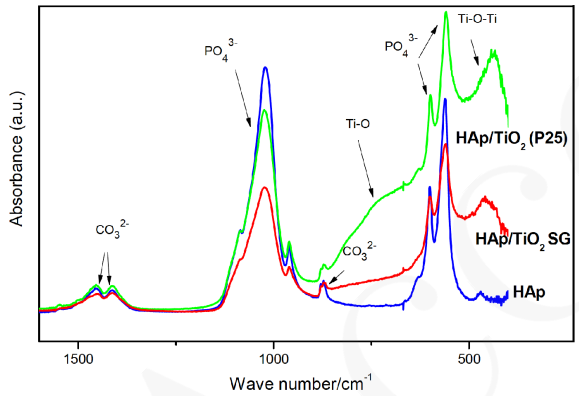

Figure 2. Characteristic infrared spectrum of HAp and HAp/TiO_2 samples

3.3. SEM

Scanning electron microscopy (SEM) technique was used to examine the morphology of the raw cuttlefish bone, hydrothermally (HT) converted cuttlefish bone and the HAp/TiO_2 composites. Also, scanning electron microscopy with energy dispersive X-ray (SEM/EDX) analysis was performed in order to confirm the presence of TiO_2 on the HAp surface.

Representative scanning electron micrographs of the raw cuttlefish bone, HAp and HAp/TiO_2 composites are shown in Fig. 3. The structure of the cuttlefish bone is systematically and in detail described by Birchall *et al.* [24]. Briefly, it consists of two regions: a thick external wall or dorsal shield and internal regions with a layered, cellular quasi-periodic microstructure consisting of lamellae separated by numerous pillars In the internal matrix, each of the individual lamellae and pillars is

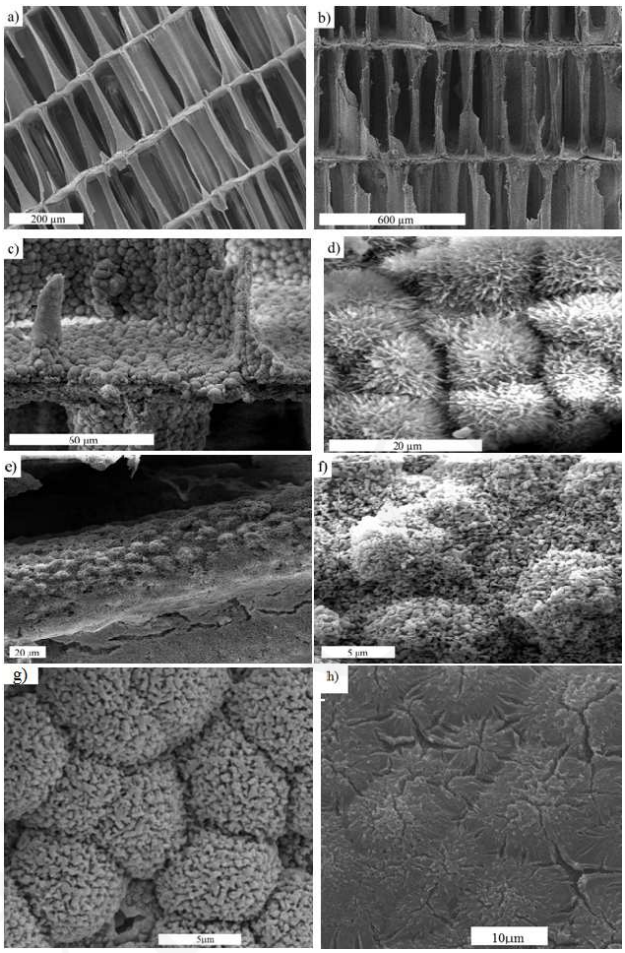

Figure 3. SEM micrographs of: a) raw cuttlefish bone after removing the organic component with NaClO, b) HAp scaffold derived from cuttlefish bone clearly displaying interconnected channeled structure maintained after HT conversion; c-d) HAp scaffold (at different magnifications) displaying HAp crystals formed on the surface of lamellae and pillars in dandelion-like (cauliflower) structures; e-f) HAp/TiO_2 (P25) obtained by impregnation of 5 wt.% TiO_2 suspension; g-h) HAp/TiO_2 SG before (g) and after calcination (h)

coated with an organic material composed primarily of β-chitin [25,26]. In order to ensure complete hydrothermal conversion of aragonite into hydroxyapatite the organic component of the cuttlefish bone was removed with an aqueous solution of sodium hypochlorite. SEM micrograph of the organic-free cuttlefish bone is shown in Fig. 3a. As shown in Fig. 3b the interconnected structure of the cuttlefish bone is completely maintained after the hydrothermal conversion into HAp. At higher magnification, irregularly shaped microspheres of HAp crystals with cauliflower morphology are formed on the surface of lamellae and pillars (Fig. 3c). The enlarged view shown in Fig. 3d indicates the existence of dandelion-like structures. These globular-shaped structures enhance the surface roughness and surface area of the HAp carrier. Figures 3e and 3f show the surface of HAp carrier impregnated with 5% TiO_2 suspension in isopropanol. Comparing Fig. 3d and Fig. 3f visible changes in the microstructure of the surface can

be observed. In the HAp/TiO_2 (P25) composite hydroxyapatite globular-shaped structures were not clearly expressed as in the HAp carrier, indicating the precipitation of the TiO_2 particles on their surface. Figures 3g and 3h show SEM images of TiO_2 layer prepared by sol-gel process, taken before and after calcination, respectively. Dandelion-like structures of HAp shown in Fig. 3d are not visible in Fig. 3g. As can be seen in Fig. 3h, cracks are formed in TiO_2 film during thermal treatment.

The presence of the TiO_2 layer on the surface of HAp carrier was confirmed by SEM microscopy with energy dispersive X-rays (SEM/EDX) (figure not shown). Analysis showed the presence of elements with a molar proportion of Ca (55.1%), O (32.3%), P (4.7%), C (0.8%), and Ti (7.0%), confirming the presence of the TiO_2 layer on the surface of HAp carrier.

3.4. BET

The quantification of mesoporosity and microporosity was carried out according to BET method by N_2 adsorption-desorption isotherms at liquid N_2 temperature. The BET surface areas, average pore diameter and total pore volume of the samples before and after calcination at 500 °C for 1 h are shown in Table 2.

From the obtained BET data it is evident that the thermal treatment of the HAp carrier at 500 °C for 1 h resulted in a decrease of the specific surface area and the size of the pores, compared to the uncalcined (dried) samples. The deposition of TiO_2 (P25) nanoparticles onto the surface of the HAp carrier resulted in the increase of the specific surface area of the samples, both, uncalcined and calcined at 500 °C, from 21.7 m^2/g to 30.4 m^2/g and from 15.7 m^2/g to 29.1 m^2/g, respectively. Also, the TiO_2 layer on the surface of HAp has led to some reduction in the pore size compared to HAp. After the calcination of the HAp/TiO_2 (P25) samples, no significant changes in the specific surface area and pore size were observed. The sample HAp/TiO_2 SG, where the TiO_2 was formed on the surface of HAp by sol-gel method and calcined at 500 °C for 1 h, showed almost identical values of S_{BET}, mean pore size and total pore volume to those of the HAp/TiO_2 (P25) analogue.

3.5. Photocatalytic properties

The photocatalytic properties of HAp/TiO_2 samples was studied by exposing the salicylic acid aqueous solution to UV light in the absence and in the presence of suspended pure TiO_2 (P25), suspended pure HAp or HAp supported TiO_2 photocatalysts.

The efficiency of the salicylic acid mineralization was evaluated by measuring the total organic carbon (TOC). The obtained results are shown in Fig. 4. and Table 3. Figure 4 shows the relative concentration of salicylic acid as a function of irradiation time. The plot of natural logarithm of relative concentration vs. irradiation time (Fig. 5) gives straight line in all the cases indicating that the photocatalytic degradation of salicylic acid is of pseudo first order:

$$\ln \frac{C}{C_0} = -k \cdot t \tag{1}$$

C_0 and C represent the initial concentration of the salicylic acid in solution and the one after a given irradiation time, t, respectively. The apparent rate constants, k, are summarized in Table 3.

As shown in Fig. 4 the salicylic acid undergoes negligible degradation under direct UV irradiation in the absence of catalyst. No change in the salicylic acid concentration during UV irradiation in the presence of suspended pure HAp was observed. As shown in Table 3, after 120 min of UV irradiation the salicylic acid removal reached 65% in the presence of suspended pure TiO_2 (P25) nanopowder, 58% in the presence of HAp/TiO_2 (P25) photocatalyst and 61% in the presence of HAp/TiO_2 SG photocatalyst prepared by sol-gel process. HAp/TiO_2 (P25) photocatalyst showed slightly lower activity in the second photodegradation cycle (HAp/TiO_2 (P25) II) compared to the first cycle, but

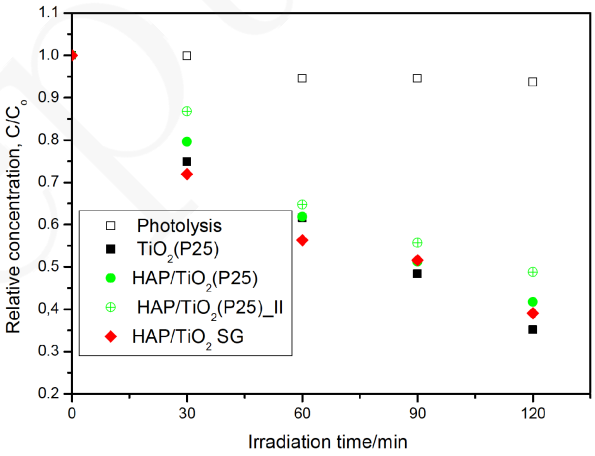

Figure 4. Photodegradation of salicylic acid in the absence (photolysis) and in the presence of catalysts: Relative concentration as a function of irradiation time

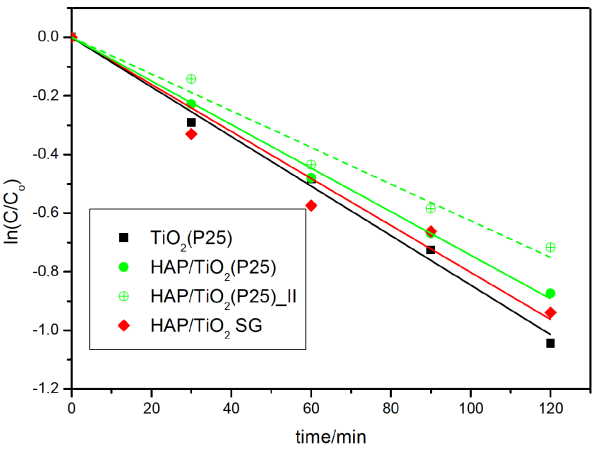

Figure 5. Pseudo first order kinetics for salicylic acid photocatalysed degradation

Table 2. Specific surface area (S_{BET}), mean pore size and total pore volume of the samples

Sample	S_{BET} [m^2/g]	Mean pore size [nm]	Total pore volume [cm^3/g]
HAp, 105 °C	21.7	21.3	0.1153
HAp	15.7	18.5	0.0727
HAp/TiO_2 (P25), 105 °C	30.4	15.8	0.1204
HAp/TiO_2 (P25)	29.1	14.4	0.1046
HAp/TiO_2 SG	29.2	14.5	0.1062

Table 3. Comparison of photocatalytic activity of catalysts for the degradation of salicylic acid (SA)

Catalyst	SA removal after 2 h of irradiation [%]	Apparent rate constants of SA degradation, k [min^{-1}]	TOC removal after 2 h of irradiation [%]
TiO_2 (P25)	65	0.00846	28
HAp/TiO_2 (P25)	58	0.00725	32
HAp/TiO_2 (P25) II	51	0.00626	36
HAp/TiO_2 SG	61	0.00802	23

it was the most efficient in the salicylic acid mineralization. It is important to note that in the investigated systems with HAp supported catalysts the quantity of the active TiO_2 phase is about two times larger compared to the system with unsupported TiO_2 catalyst. It is obvious that immobilization of catalyst does result in a loss of its activity. However, the supported catalysts have the advantage that they can be easily separated from the reaction mixture and reused. TiO_2 suspension in water presents a highly stable hydrocolloid [27] which makes the separation of catalyst from water and its re-application difficult.

The slightly higher efficiency in the salicylic acid removal of HAp/TiO_2 SG, compared to the HAp/TiO_2 (P25) photocatalyst, could be attributed to the larger quantity of anatase phase in the TiO_2 layer and smaller nanosized particles increasing specific surface area.

The apparent rate constants, k, are in the same order of magnitude (Table 3). The values of k for the degradation of salycilic acid in the presence of HAp supported photocatalysts are slightly lower than that for the degradation in the presence of suspended pure TiO_2 (P25) photocatalyst.

From all results we can conclude that the highly porous 3D HAp support prepared in this work ensure a large surface area of immobilized catalyst and have a potential for photocatalytic applications. The macrochannels in the structure serve as effective paths for light and ensure good mass transport of the pollutants to the catalyst surface.

Use of natural marine resources and residues such as cuttlefish bones and their conversion into highly added value products such as catalyst support, simple preparation route and easy separation from reaction mixture make the prepared catalysts economic and environmentally friendly materials. The development and findings of the present work can be readily extended to other catalyst immobilization systems.

IV. Conclusions

Porous hydroxyapatite/titania (HAp/TiO_2) composites were synthesized by simple and cost-effective routes. TiO_2 was deposited on the pore walls of the highly porous HAp support derived from cuttlefish bone using vacuum impregnation and sol-gel technique. A homogeneous distribution of TiO_2 particles covering the surface of the HAp was achieved. The photocatalytic activity of the prepared materials was studied using salicylic acid as a model water pollutant and it was found comparable to that of suspended TiO_2 nanoparticles.

Acknowledgement: This work has been supported in part by the Croatian Science Foundation under the project IP-2014-09-3752.

References

1. Z.R. Ismagilov, R.A. Shkrabina, N.A. Koryabkina, A.A. Kirchanov, H. Veringa, P. Pex, "Porous alumina as a support for catalysts and membranes. Preparation and study", *React. Kinet. Catal. Lett.*, **60** [2] (1997) 225–231.
2. W.H. Cassinelli, L. Martins, A.R. Passos, S.H. Pulcinelli, A. Rochet, V. Briois, C.V. Santilli, "Correlation between structural and catalytic properties of copper supported on porous alumina for the ethanol dehydrogenation reaction", *Chem. Cat. Chem.*, **7** [11] (2015) 1668–1677.
3. Z. Fu, J. Xie, F. He, F. Fang, "Synthesis of porous cordierite and application for MnO_x/TiO_2 catalyst support", *Russ. J. Appl. Chem.*, **87** [1] (2014) 1749–1754.
4. R.J. Davis, "New perspectives on basic zeolites as catalysts and catalyst supports", *J. Catal.*, **216** [1-2] (2003) 396–405.
5. C. Duong-Viet, H. Ba, Z. El-Berrichi, J.-M. Nhut, M.J. Ledoux, Y. Liu, C. Pham-Huu, "Silicon carbide foam as a porous support platform for catalytic applications", *New. J. Chem.*, **40** [5] (2016) 4285–4299.
6. V.G. Deshmane, S.L. Owen, R.Y. Abrokwah, "Mesoporous nanocrystalline TiO_2 supported metal (Cu, Co, Ni, Pd, Zn, and Sn) catalysts: Effect of metal-support interactions on steam reforming of methanol", *J. Mol. Catal. A - Chem.*, **408** (2015) 202–213.
7. X.P. Zhang, Q.D. Zhang, N. Tsubaki, Y. Tan, Y. Han, "Car-

bon dioxide reforming of methane over Ni nanoparticles incorporated into mesoporous amorphous ZrO_2 matrix", *Fuel*, **147** (2015) 243–252.
8. N. Phonthammachai, Z. Ziyi, G. Jun, H.Y. Fan, T.J. White, "Synthesis of high performance hydroxyapatite-gold catalysts for CO oxidation", *Gold Bull.*, **41** [1] (2008) 42–50.
9. R. Radhakrishnan, K. Kannan, S. Kumaravel, S. Thiripuranthagan, "Oxidative esterification of furfural over Au-Pd/HAP-T and Au-Ag/HAP-T bimetallic catalysts supported on mesoporous hydroxyapatite nanorods", *RSC Adv.*, **6** [51] (2016) 45907–45922.
10. R. Chakraborty, D. RoyChowdhury, "Optimization of biological- hydroxyapatite supported iron catalyzed methyl oleate synthesis using response surface methodology", *J. Taiwan Inst. Chem. Eng.*, **45** [1] (2014) 92–100.
11. R. Chakraborty, D. RoyChowdhury, "Fish bone derived natural hydroxyapatite-supported copper acid catalyst: Taguchi optimization of semibatch oleic acid esterification", *Chem. Eng. J.*, **215** (2013) 491–499.
12. R. Chakraborty, S.K. Das, "Optimization of biodiesel synthesis from waste frying soybean oil using fish scale-supported Ni catalyst", *Ind. Eng. Chem. Res.*, **51** [25] (2012) 8404–8414.
13. T. Szatkowski, K. Siwińska-Stefańska, M. Wysokowski, A.L. Stelling, Y. Joseph, H. Ehrlich, T. Jesionowski, "Immobilization of titanium(IV) oxide onto 3D spongin scaffolds of marine sponge origin according to extreme biomimetics principles for removal of C. I. basic blue 9", *Biomim.*, **2** (2017) 4.
14. H. Ivanković, G. Gallego Ferrer, E. Tkalčec, S. Orlić, M. Ivanković, "Preparation of highly porous hydroxyapatite from cuttlefish bone", *J. Mater. Sci.: Mater. Med.*, **20** (2009) 1039–1046.
15. D. Milovac, G. Gallego Ferrer, M. Ivanković, H. Ivanković, "PCL-coated hydroxyapatite scaffold derived from cuttlefish bone: morphology, mechanical properties and bioactivity", *J. Mater. Sci. Eng. C*, **34** (2014) 437–445.
16. D. Milovac, T.C. Gamboa-Martinez, M. Ivanković, G. Gallego Ferrer, H. Ivanković, "PCL-coated hydroxyapatite scaffold derived from cuttlefish bone: In vitro cell culture studies", *J. Mater. Sci. Eng. C*, **42** (2014) 264–272.
17. Y. Tao, C.-Y. Wu, D.W. Mazyck, "Microwave-assisted preparation of TiO_2/activated carbon composite photocatalyst for removal of methanol in humid air streams", *Ind. Eng. Chem. Res.*, **45** (2006) 5110–5116.
18. D. Kibanova, J. Cervini-Silva, H. Destaillats, "Efficiency of clay-TiO_2 nanocomposites on the photocatalytic elimination of a model hydrophobic air pollutant", *Environ. Sci. Technol.*, **43** (2009) 1500–1506.
19. C.H. Ao, S.C. Lee, "Indoor air purification by photocatalyst TiO_2 immobilized on an activated carbon filter installed in an air cleaner", *Chem. Eng. Sci.*, **60** (2005) 103–109.
20. M.R. Samarghand, J. Nouri, A.R. Mesdaghinia, A.H. Mahvi, S. Nasseri, F. Vaezi, "Efficiency removal of phenol, lead and cadmium by means of UV/TiO_2/H_2O_2 processes", *Int. J. Environ. Sci. Technol.*, **4** (2007) 19–25.
21. X. Meng, Z. Qian, H. Wang, X. Gao, S. Zhang, M. Yang, "Sol-gel immobilization of SiO_2/TiO_2 on hydrophobic clay and its removal of methyl orange from water", *J. Sol-Gel Sci. Technol.*, **46** (2008) 195–200.
22. E. Landi, G. Celotti, G. Logroscino, A. Tampieri, "Carbonated hydroxyapatite as bone substitute", *J. Eur. Ceram. Soc.*, **23** [15] (2003) 2931–2937.
23. A. Saranya, J. Pandiarajan, N. Prithivikumaran, "Synthesis and characterization of TiO_2/PS nano structure for sensor applications", *Inter. J. Techn. Res. Appl.*, **38** (2016) 57–60.
24. J.D. Birchall, N.L. Thomas, "On the architecture and function of cuttlefish bone", *J. Mater. Sci.*, **18** (1983) 2081.
25. G. Falini, S. Fermani, "Chitin mineralization", *Tissue Eng.*, **10** [1-2] (2004) 1–6.
26. J. Cadman, S.W. Zhou, Y.H. Chen , Q. Li, "Cuttlebone: characterisation, application and development of biomimetic materials", *J. Bionic Eng.*, **9** (2012) 367–376.
27. P. Ciambelli, D. Sannino, M. Sarno, "Nanocatalysts: A new "dimension" for nanoparticles?", pp. 511–546 in *Inorganic Nanoparticles: Synthesis, Applications, and Perspectives*. Eds. C. Altavilla, E. Ciliberto, CRC Press, Boca Raton, 2011.